Migration energies in $L1_2$ intermetallic compounds

2000 J. Phys.: Condens. Matter 12 8145

(http://iopscience.iop.org/0953-8984/12/37/313)

J. Phys.: Condens. Matter **12** (2000) 8145–8158. Printed in the UK PII: S0953-8984(00)10732-5

Migration energies in $L1_2$ intermetallic compounds

E Kentzinger and H R Schober

Institut für Festkörperforschung, Forschungszentrum Jülich, D-52425 Jülich, Germany

Received 6 January 2000, in final form 5 May 2000

Abstract. The migration energies E_M for the jumps into nearest-neighbour vacancies in $L1_2$ intermetallic compounds are related to the static lattice Green functions that can be calculated from the measured phonon dispersions. The present approach is an extension of a similar approach used earlier for BCC and FCC pure metals (Schober H R, Petry W and Trampenau J 1992 *J. Phys.: Condens. Matter* **4** 9321). In A_3B compounds with the $L1_2$ structure, three first-nearest-neighbour jumps into vacancies have to be distinguished and in some cases there is a bias, ΔE, between final and initial configurations. As was done earlier for monatomic lattices by Schober *et al*, the migration energy is split into two terms, one depending only on structure and a material-dependent term, given by the Green function elements. The difference in size between A and B atoms has to be taken into account and the compounds have to be separated into two groups depending on the size of the majority atoms relative to the minority ones. The formulae have been checked by computer simulations. The values of E_M or $E_M - \Delta E/2$ are calculated for those $L1_2$ compounds where the phonon dispersions have been measured. In the case of the Ni_3Al system, other theoretical and experimental determinations compare well with our model. Comparing these energies with the critical temperatures of stability of the $L1_2$ structure, we note a significant contribution of the ordering energy to the migration energy for all three jump types.

1. Introduction

Among the three energetic parameters that drive self-diffusion and ordering kinetics in ordered intermetallic compounds, i.e. the activation (E_A), the formation (E_F) and the migration (E_M) energies, the latter one is experimentally least well known and hardest to measure [1]. E_M has been determined directly for B2-ordered compounds at high temperatures by positron lifetime measurements (FeAl [2, 3] and NiAl [4]) and by length change studies (FeAl and NiAl [5], NiGa and CoGa [6]) of the equilibration process of thermal vacancies during a temperature change. In compounds exhibiting other structures (DO_3, $L1_2$, DO_{19}), direct determinations are scarce and E_M was in some cases deduced from the difference between E_A (from self-diffusion or ordering kinetics) and E_F (from positron lifetime spectroscopy) [1]. To the authors' knowledge, direct determinations of the migration energies in those structures exist only in the cases of $L1_2$-Ni_3Al [7] and DO_3-Fe_3Al [3], deduced from measurements of recovery after electron irradiation or quenching by means of positron annihilation studies. Moreover, all the migration barriers were averaged over both species and over their respective initial and final sublattices.

Recently, a model relating the migration energy for vacancies in cubic metals to the phonon dispersion has been proposed by one of the present authors [8]. This model follows the earlier ideas of Herzig [9] to explain the fast diffusion in BCC metals by the presence of

0953-8984/00/378145+14$30.00

soft phonon modes. In this model, the migration energy E_M is estimated from the following relation:

$$E_M = \alpha G_0^{-1} a^2 \qquad \text{where } G_0 = \int \frac{Z(\omega)}{M\omega^2}\, \mathrm{d}\omega. \tag{1}$$

In this equation, E_M is separated into a structural term (α), common to all FCC or BCC metals, and a term (G_0), the static lattice Green function, which is the ω^{-2}-moment of the normalized phonon density of states $Z(\omega)$. It is due to this ω^{-2}-weighting that low-energy phonons are the essential quantities for probing the migration barrier. a is the lattice parameter and M the atomic mass. $\alpha_{\mathrm{FCC}} = 0.0135(7)$ and $\alpha_{\mathrm{BCC}} = 0.0130(7)$ have been found from molecular statics simulations. This model extends the earlier model of Flynn [10] who related E_M to the elastic constants, i.e. the continuum limit of the phonon spectrum.

In the high-temperature approximation the mean square displacement, which is inversely proportional to the curvature of the equilibrium potential of the perfect lattice, can be expressed as $\langle u_x^2 \rangle = k_B T G_0$ (see e.g. [11]) which shows, together with equation (1), that, at a certain temperature T, E_M is related to the curvature of this equilibrium potential.

For FCC metals excellent agreement between the calculated and measured values of E_M was found. For BCC metals, where experimental values are less well known, the predictions show pronounced group systematics. More recently, the same *ansatz* was used to estimate the *mean* migration barriers in the DO_3-ordered compounds Fe_3Si [12], Ni_3Sb [13] and Fe_3Al [14] which show fast diffusion or small activation energies of ordering kinetics. For DO_3-Fe_3Al, a value of 0.5 eV was found, in good agreement with another direct experimental determination based on positron annihilation studies [3]. Those studies helped their authors to deduce that fast atomic mobility in DO_3 intermetallics results from the combination of low migration barriers and high vacancy concentrations [14, 15].

The purpose of the present paper is to find relations similar to equation (1) for first-nearest-neighbour vacancy jumps in intermetallic compounds of the $L1_2$ structure. This structure (also called Cu_3Au structure) is an ordered phase on the FCC lattice. As shown schematically in figure 1, in such an A_3B compound the A atoms occupy the face centres (the α-sublattice) and the B atoms occupy the cube corners (β-sublattice). This different occupation has important consequences. First, there are two different types of vacancy and two different types of anti-site defect. Consequently, starting from the fully ordered state with one vacancy, three first-nearest-neighbour jumps into this vacancy can be distinguished (see figure 2): the jump of an atom of type A in the α-sublattice into a vacancy (V) in the same sublattice ($A_\alpha \rightarrow V_\alpha$), the jump of an A atom in the α-sublattice into a vacancy in the β-sublattice ($A_\alpha \rightarrow V_\beta$) and the jump of a B atom in sublattice β into a vacancy in the α-sublattice ($B_\beta \rightarrow V_\alpha$). Secondly, the symmetry

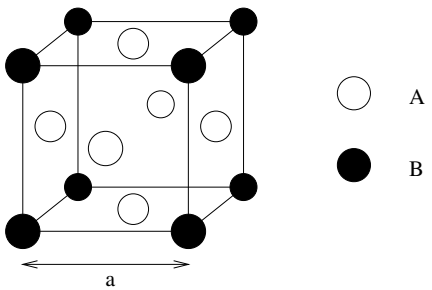

Figure 1. The $L1_2$ structure. A and B atoms occupy the α- and β-sublattices, respectively. a is the lattice parameter. For the purpose of perspective, the atoms belonging to more distant planes are represented by smaller circles.

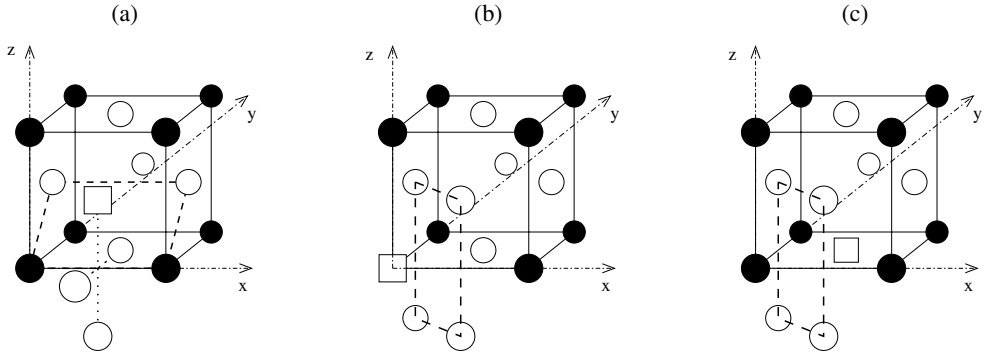

Figure 2. Starting positions for the three inequivalent first-nearest-neighbour atom jumps into a vacancy (represented here as a square). The atoms, forming the barrier of first-nearest neighbours that the jumping atom has to overcome, are connected by a dashed line. (a) The jump of atom A at (0.5, 0.5, 0.0) in the α-sublattice into a vacancy at (0.5, 0.0, 0.5) in the same sublattice (the $A_\alpha \rightarrow V_\alpha$ jump). The two atoms connected to the jumping atom and the vacancy by dotted lines are the ones that prevent the migrating atom from straying too far off the straight line in the case of $\Delta > 0$ in subsection 3.3. (b) The jump of atom A at (0.5, 0.5, 0.0) in the α-sublattice into a vacancy at (0, 0, 0) in the β-sublattice (the $A_\alpha \rightarrow V_\beta$ jump). (c) The jump of atom B at (0, 0, 0) in the β-sublattice into a vacancy at (0.5, 0.5, 0.0) in the α-sublattice (the $B_\beta \rightarrow V_\alpha$ jump). The coordinates are given in units of the lattice parameter a.

along the reaction path is reduced compared to that of the FCC lattice which can lead to deviations from the straight line connecting initial and final positions of the jumping atom.

The main aim of this work is to check how, for each of the three jump types mentioned above, the migration energy can be related to the Green function matrix for atoms A and B analogously to equation (1), i.e. via a relation common to all $L1_2$ compounds. Due to the difference between the sublattices, the split of the migration energy into two terms, namely a material-independent term and one given by the Green function matrix elements of the constituent atoms, will not be so straightforward and will have to account for the differences between A and B atoms, leading e.g. to a curved path or a bias between the initial and final configurations of the jump considered. Furthermore, we will have to account for the type of neighbour (A or B) that the atom will be in contact with during the jump. The response of the lattice will be different for 'large' and 'small' vacancies. We will show that the compounds have to be separated into two groups, depending on the relative strengths of the repulsion between pairs of different atoms, with the result that the relations found for one group differ slightly from those for the other.

An important point is that, for two of the jumps (namely $A_\alpha \rightarrow V_\beta$ and $B_\beta \rightarrow V_\alpha$), the energy of the lattice after the jump differs from that before. Let us call this bias ΔE. We will show that, depending on which of the two above-mentioned groups the compound considered belongs to, the Green function gives either the migration energy itself or a combination of the migration energy and ΔE.

This paper is organized as follows. In section 2, we recall some general features of the static lattice Green function formalism and show how this function can be calculated from the phonon dispersion. Section 3 is devoted to the development of the model giving access to the migration energy for the three nearest-neighbour jumps. The molecular static calculation procedure and the potentials used to verify the model are described in section 4. In section 5, the migration energies are calculated and discussed for compounds whose phonon dispersions have been measured. Conclusions are drawn in section 6.

2. The static lattice Green function

The static lattice Green function is an important tool in the calculation of the properties of lattices with defects [16]. It is especially useful for calculating the response of the full lattice to forces on single atoms. If one exerts a static force $\boldsymbol{F}^m$ on atom m, the displacement of this atom from its equilibrium position in an infinite lattice is given by

$$\boldsymbol{r}^m = \mathbf{G}^{mm}\boldsymbol{F}^m \tag{2}$$

where $\mathbf{G}^{mm}$ is the static lattice Green function matrix of atom m. All of the other atoms will relax in order to minimize the elastic energy to a value of

$$E_{el} = \frac{1}{2}\boldsymbol{F}^m\mathbf{G}^{mm}\boldsymbol{F}^m. \tag{3}$$

Inverting equation (2) to $\boldsymbol{F}^m = (\mathbf{G}^{mm})^{-1}\boldsymbol{r}^m$ the energy of the relaxed lattice can be written in terms of the displacements:

$$E_{el} = \frac{1}{2}\boldsymbol{r}^m(\mathbf{G}^{mm})^{-1}\boldsymbol{r}^m. \tag{4}$$

In a perfect lattice, the Green function matrix elements G_{ij}^{mm} ($i, j = x$, y or z) can be expressed in terms of the eigenvalues $\omega^s(\boldsymbol{q})$ and eigenvectors (i.e. polarization vectors) $e^s(\boldsymbol{q})$ ($s = 1, \ldots, 3n$ where n is the number of atoms in the unit cell) of the dynamical matrix at wave vector $\boldsymbol{q}$ which are known from fits (e.g. Born–von Karman) to the measured phonon dispersion:

$$G_{ij}^{mm} = \int \frac{Z_{ij}^{mm}(\omega)}{M^m\omega^2}\,\mathrm{d}\omega \tag{5}$$

where M^m is the mass of atom m and $Z_{ij}^{mm}(\omega)$ is the partial phonon density of states:

$$Z_{ij}^{mm}(\omega) = \frac{1}{3n}\frac{V}{(2\pi)^3}\sum_s \int e_i^{m,s}(\boldsymbol{q})e_j^{m,s}(\boldsymbol{q})\delta(\omega - \omega_s(\boldsymbol{q}))\,\mathrm{d}\boldsymbol{q}. \tag{6}$$

V is the volume of the unit cell and the integration extends over the first Brillouin zone. In the case of a monatomic FCC or BCC metal, $\mathbf{G}^{mm}$ is diagonal and reduces to one number, G_0, proportional to the ω^{-2}-moment of the phonon spectrum (see equation (1)).

In an A_3B compound with the $L1_2$ structure, atom B also has cubic point symmetry and its Green function matrix $\mathbf{G}^{BB}$ reduces also to one number, G_{xx}^{BB}. The point symmetry of the A atoms is only tetragonal. For an A atom at position (0.5, 0.5, 0.0) in the unit cell, one has

$$\mathbf{G}^{AA} = \begin{pmatrix} G_{xx}^{AA} & 0 & 0 \\ 0 & G_{xx}^{AA} & 0 \\ 0 & 0 & G_{zz}^{AA} \end{pmatrix} = \tilde{\mathbf{G}}^{AA} + \begin{pmatrix} \Delta & 0 & 0 \\ 0 & \Delta & 0 \\ 0 & 0 & -\Delta \end{pmatrix} \tag{7}$$

where

$$\Delta = (G_{xx}^{AA} - G_{zz}^{AA})/2 \tag{8}$$

and $\tilde{\mathbf{G}}^{AA}$ is a diagonal matrix with elements $\tilde{G} = (G_{xx}^{AA} + G_{zz}^{AA})/2$. (Our definition of $\tilde{\mathbf{G}}^{AA}$ instead of the proper cubic average, using $\mathrm{tr}\,\mathbf{G}^{AA}/3$, avoids numerical factors in the later expressions.) The Green function matrices for the two other A atoms in the unit cell are obtained by circular permutation of the matrix elements.

We thus express the deviation from a cubic response function by a single constant, Δ, which is a measure of the relative softness. The physics behind this can be understood if one takes into account that in close-packed metallic lattices the nearest-neighbour interaction is always dominant. Let us denote the longitudinal force constants for nearest-neighbour pairs of

atoms by f^{AA} and f^{AB} for AA and AB pairs, respectively. In first-order perturbation theory, Δ is then given by

$$\Delta = (f^{AA} - f^{AB})\tilde{G}^2. \tag{9}$$

That is, it is a measure for the change in response caused by replacing a B neighbour by an A one. For convenience, we will in the following say atom A is 'larger' or 'stronger' than atom B if $\Delta > 0$.

In calculations of specific properties one has, of course, always to take care of the projection to the displacement direction. In an ideal FCC lattice a displacement in any direction will strain an effective force constant $f_{eff} = 4f$, again assuming a nearest-neighbour interaction with force constant f. For a displacement in x-, y-, z-directions this f_{eff} will be equally distributed on eight of the twelve nearest neighbours. The other four are in directions orthogonal to the displacement vector. The projection of the displacement vector onto the vector connecting the displaced atom to its neighbours gives a factor of 0.5 for each bond. For a displacement in the xy-direction one has two atoms in the displacement direction, each with a projection weight of 1. Eight other atoms contribute with a weight of 0.25, each. These different weights of the nearest-neighbour atoms will play an important role in our later considerations. It will clearly make a difference whether an atom of the first group or the second group is changed. In comparing the response in the defect lattice to the one of the ideal lattice we will have to take the nature of the defect into account (A or B vacancy). This can be done approximately by adding the appropriate Δ terms.

3. The model

The migration energy E_M is the potential energy needed to move an atom adiabatically from its initial position to a first-nearest-neighbour vacancy. We want to express this energy now in terms of the static lattice Green function, following the arguments used in reference [8] for the case of pure FCC and BCC metals. Let us first recapitulate these arguments and only later introduce the appropriate correction terms to account for the deviation of the $L1_2$ lattice from the monatomic FCC one.

3.1. The monatomic FCC lattice

In the FCC lattice the energy curve $E(\rho)$ in the reaction coordinate ρ, connecting the initial and final positions of the jumping atom, is well reproduced by a sine shape:

$$E(\rho) = \frac{1}{2}E_M\left(1 - \cos\frac{\pi\rho}{d}\right) \tag{10}$$

where d is the distance to the saddle point. For small distortions from the equilibrium positions at $\rho = 0$, equation (10) can be expanded to

$$E(\rho) = \frac{1}{2}E_M\frac{\pi^2}{2d^2}\rho^2. \tag{11}$$

Introducing a unit vector, $\boldsymbol{u}^m = \boldsymbol{r}^m/r^m$, one gets from equation (4) in conjunction with equation (11)

$$E_M = \frac{2}{\pi^2}\boldsymbol{u}^m(\mathbf{G}^{mm})^{-1}\boldsymbol{u}^m d^2. \tag{12}$$

In deriving this equation we assumed that the curvatures of the effective potential at the equilibrium and saddle-point positions are equal. This, however, is only an approximation:

usually the curvature of the potential at the saddle-point position is much smaller. Equation (12) is improved by averaging the two curvatures, i.e. by replacing $\mathbf{G}$ by the average†

$$\overline{\mathbf{G}} = \frac{1}{2}(\mathbf{G}_{equ} - \mathbf{G}_{saddle}) \tag{13}$$

where $\mathbf{G}_{equ}$ refers to a relaxed lattice around the vacancy and the jumping atom at its equilibrium position, and $\mathbf{G}_{saddle}$ refers to a lattice with the atom at the saddle point. Simulations showed that equations (12) and (13) reproduce E_M in equation (10) within a few per cent.

Unfortunately the Green functions, needed to evaluate equation (12) and (13), are not accessible experimentally. Therefore, in view of the fact that the structure of the vacancies and saddle point is not very different for different FCC metals it was then assumed that there is one structural constant connecting the ideal-lattice Green function $\mathbf{G}_0$ with the needed effective $\overline{\mathbf{G}}$. By computer simulations a relation $\overline{\mathbf{G}} \approx 1.88\mathbf{G}_0$ was found. Using $d = \sqrt{2}/4a$ and combining the numerical factors, one thus arrives at equation (1). As was shown in the simulations, equation (10) together with equations (12) and (13) describes the potential energy along the action path within a few per cent. If one took a somewhat different analytic form, there would be a shift between the geometrical factors in equation (12) and the factor 1.88. The factor α finally used in equation (1) would, however, remain unchanged.

3.2. $L1_2$ compounds

As long as the two species A and B have similar properties, equation (1) can be used as a suitable zero-order approximation for the $L1_2$ compounds also. The Green function element can then be calculated, e.g. from an average phonon dispersion. This has been done for $B2$ and DO_3 compounds ordered on a BCC lattice [12–14]. Since, however, sometimes the exact dispersion curves are also available, we want to utilize them to calculate, to first order in Δ (equation (8)), the migration energies of the individual atoms.

In general, in the compounds, the energies after and before the jump are not equal. Let us denote this difference by ΔE. The potential energy curve equation (10) then has to be amended by adding a linear term:

$$E(\rho) = \frac{1}{2}E_a\left(1 - \cos\frac{\pi\rho}{d}\right) + \frac{\Delta E}{\Delta\rho}\rho \tag{14}$$

where $E_a = E_M - \Delta E/2$ and $2d$ is again the distance between the two minima. As in the monatomic case, the energy curves found in the simulations can be fitted within a few per cent by this expression. In analogy to the results for monatomic FCC metals, one would expect equation (1) with the appropriate Green function terms to give an estimate for E_a. We find this for the case of smaller majority atoms ($\Delta < 0$). In the opposite case, however, the migration energy E_M is gained. The reason for this dependence on the size bias will be given in subsection 3.4.

Following the arguments used above for the monatomic FCC lattice it becomes clear that different Green function elements will contribute to the three different vacancy jumps shown in figure 2. In the case of the $A_\alpha \rightarrow V_\alpha$ jump the jump path is no longer determined by symmetry. The jumping A atom will preferentially follow a curved path if this helps to avoid a stiff direction. The direction of minimal-energy motion can be estimated from the two Green function elements in question and the effective curvature can then be taken into account. Furthermore, the vacancy can be larger or smaller than the 'average' one. This means,

† In reference [8] we used the average $\overline{\mathbf{G}^{-1}} = \frac{1}{2}(\mathbf{G}^{-1}_{equ} - \mathbf{G}^{-1}_{saddle})$. The average in equation (13) gives better agreement in the case of very strong differences between equilibrium and saddle-point curvatures.

compared to the ideal lattice, less or more repulsion has been taken out. In first order this can be accounted for by adding or subtracting a term proportional to Δ, defined in equation (8).

A more serious difficulty stems from the asymmetry of the reaction of the close-packed lattice to 'small' and 'large' defects. This is seen in the small relaxation volume of vacancies (the smallest substitutional defect) [17, 18]. The close packing prevents the collapse of the vacancy. Introducing a big defect on the other hand causes an opening up and the lattice can react. The short-range structure is dominated by the nearest-neighbour repulsion. The balancing attractive forces are more long ranged and therefore less structure selective. We observe a similar scenario also in our simulations of the $L1_2$ lattice; see the next section. A lattice where the majority (A) atoms are large reacts differently to a lattice where they are small. The first case corresponds to 'small' defects (B atoms), the second one to large defects. This means that for each of the three jumps we will have to distinguish between $\Delta > 0$ and $\Delta < 0$.

The programme is therefore as follows. First we determine which type of atom the moving atom encounters in its jump. This determines the combination of Green function elements entering our formulae. Additionally we have to look for blocking effects of 'large' atoms. The resulting formulae will then be tested by simulations in the next section. Details of the derivation of the formulae are given in the following subsections, separately for each case.

3.3. The jump $A_\alpha \rightarrow V_\alpha$

In this case the jump does not involve a change of sublattice, and, therefore, the energy difference $\Delta E = 0$. The jump path (path of minimal energy) is not fully determined by symmetry. To jump into a nearest-neighbour vacancy in the α-sublattice, atom A has to overcome a barrier formed by its nearest neighbours, namely two atoms A and two atoms B (see figure 2(a)), placed such that the lowest-energy path of the jumping atom towards the vacancy is curved. The curvature of this path obviously depends on the sign of Δ. Figure 3 shows this for an example from our simulations, discussed in the following section.

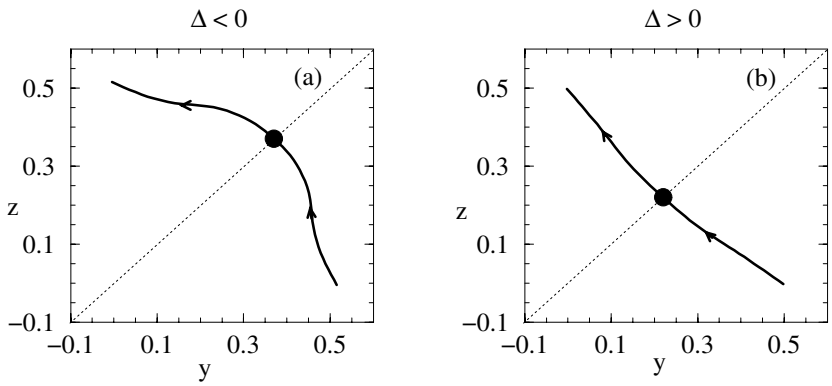

Figure 3. Examples of the paths (solid lines) in the $x = 0.5$ plane of an atom A from its equilibrium position near (0.5, 0.5, 0.0) to a nearest-neighbour vacancy in the α-sublattice near (0.5, 0.0, 0.5) and positions of the saddle point (filled circles). The coordinates are in units of the lattice parameter a. The coordinate of the saddle point is (0.5, η, η) with $\eta > 0.25$ (<0.25) when $\Delta < 0$ (>0). (a) $\Delta < 0$ ($G_{xx}^{AA} = 1.263 \times 10^{-2}$ m N^{-1}; $G_{zz}^{AA} = 2.201 \times 10^{-2}$ m N^{-1}). The actual value of η is 0.37. Equation (15) gives $\eta = 0.32$. (b) $\Delta > 0$ ($G_{xx}^{AA} = 1.106 \times 10^{-2}$ m N^{-1}; $G_{zz}^{AA} = 0.894 \times 10^{-2}$ m N^{-1}). The actual value of η is 0.22. Equation (17) gives $\eta = 0.23$ and $\eta = 0.25$, respectively, in linear approximation.

Let us take first the case $\Delta < 0$, i.e. the A atoms are the less repulsive ones. The jump path for the smaller majority atoms will avoid the larger minority atoms, i.e. the saddle-point path will be bent away from the two B atoms of the barrier towards the two A atoms. Since this brings the atom into contact again with A atoms it is not strongly inhibited by these further neighbours. The position of the saddle point can be approximately calculated using the elements of $\mathbf{G}^{\mathrm{AA}}$. Using equation (12) one can easily show that its coordinates are, in units of the lattice parameter,

$$(0.5, \eta, \eta) \qquad \text{where } \eta = \frac{G_{xx}^{\mathrm{AA}\,-1}}{2(G_{xx}^{\mathrm{AA}\,-1} + G_{zz}^{\mathrm{AA}\,-1})} \approx 0.25\left(1 - \frac{\Delta}{\tilde{G}}\right) \qquad (\Delta < 0) \tag{15}$$

where we neglected, as in the following, terms of order Δ^2. From figure 3(a) one sees that equation (15) describes the initial direction of the path. It underestimates the displacement from the straight path near the saddle point. In the example, the difference between atoms A and B is so large that the saddle point is more than the nearest-neighbour distance away from the ideal position of the nearest B atom.

Approximating the curved path to the saddle point by a straight line connecting the equilibrium position before the jump approximately at (0.5, 0.5, 0.0) to the approximate position of the saddle point at (0.5, η, η), we get in analogy to equation (1) for the migration energy

$$E_M(\mathrm{A}_\alpha \to \mathrm{V}_\alpha) = \alpha_{\mathrm{FCC}} \boldsymbol{u} (\mathbf{G}^{\mathrm{AA}})^{-1} \boldsymbol{u} a^2 \approx \alpha_{\mathrm{FCC}} \tilde{G}^{-1} a^2 \qquad (\Delta < 0) \tag{16}$$

where $\boldsymbol{u}$ is the unit vector in the direction $(0, \eta - 0.5, \eta)$. This simple final expression is formally equal to equation (1). In fact the energy gain due to the curved path compensates for the energy penalty that would have to be paid for jumping into a vacancy smaller than the 'average' one.

In the opposite case ($\Delta > 0$), when the A–A repulsion is stronger than the A–B one, this equation no longer holds. The path that would be given by equation (15) is blocked by the rigidity of the lattice of large majority atoms. The curvature of the trajectory of atom A is reduced by the two other atoms A at the positions (0.5, 0.0, -0.5) and (0.5, -0.5, 0.0). These two atoms (represented in figure 2(a)) prevent the trajectory from straying too far off the straight line. The distance to these second-nearest neighbours of the vacancy and of the jumping atom is, even for a straight path, only 10% above the nearest-neighbour distance. Any strong curvature would, therefore, bring the jumping atom into close contact with these large atoms. This can be taken into account by adding a term $\Delta\mathbf{I}$ to $\mathbf{G}^{\mathrm{AA}}$ in equation (15), where $\mathbf{I}$ is the unit matrix:

$$\eta = \frac{(G_{xx}^{\mathrm{AA}} + \Delta)^{-1}}{2[(G_{xx}^{\mathrm{AA}} + \Delta)^{-1} + (G_{zz}^{\mathrm{AA}} + \Delta)^{-1}]} \approx 0.25 \qquad (\Delta > 0). \tag{17}$$

In lowest order in Δ the jump path is a straight line, connecting the initial and final positions. This finding is again in agreement with the simulation results; see figure 3(b).

To estimate the migration energy we can now directly apply equation (12) for the ideal FCC lattice and only have to correct for the size of the vacancy by adding the correction term Δ, giving

$$E_M(\mathrm{A}_\alpha \to \mathrm{V}_\alpha) = \alpha_{\mathrm{FCC}} \boldsymbol{u} (\mathbf{G}^{\mathrm{AA}} + \Delta\mathbf{I})^{-1} \boldsymbol{u} a^2 \approx \alpha_{\mathrm{FCC}} \tilde{G}^{-1} \left(1 - \frac{\Delta}{\tilde{G}}\right) a^2 \qquad (\Delta > 0). \tag{18}$$

The migration energy is given as in an ideal average lattice corrected by a bonus for jumping into a large vacancy.

3.4. The jump $A_\alpha \rightarrow V_\beta$

Contrary to the case for the previously discussed jump, here and in the following subsection, for the jumps involving a change of sublattice, in general ΔE is no longer equal to zero.

To jump into a nearest-neighbour vacancy at position (0, 0, 0) in sublattice β, the atom A at position (0.5, 0.5, 0.0) in sublattice α has to overcome a barrier formed by its nearest neighbours, four atoms of type A. The path of minimal energy is straight due to symmetry. To apply equation (12) we have to determine the appropriate elements of the Green function. The barrier is composed of four atoms A. This corresponds to the direction z in the ideal lattice, i.e. the appropriate element is G^{AA}_{zz}. The size of the vacancy again is accounted for by an extra Δ giving $G^{\mathrm{AA}}_{zz} + \Delta = \tilde{G}$. We thus get the simple result

$$E_M(\mathrm{A}_\alpha \rightarrow \mathrm{V}_\beta) = \alpha_{\mathrm{FCC}} \boldsymbol{u}[(G^{\mathrm{AA}}_{zz} + \Delta)\mathbf{I}]^{-1}\boldsymbol{u}a^2 \approx \alpha_{\mathrm{FCC}}\tilde{G}^{-1}a^2 \qquad (\Delta > 0) \tag{19}$$

where $\boldsymbol{u} = (1, 1, 0)/\sqrt{2}$. It is somewhat surprising that equation (19) gives the migration energy directly and not, as one might expect from equation (14), $E_M - \Delta E/2 = E_a$. This result which we first saw in our simulations is, as mentioned above, a result of the relative rigidity of the $L1_2$ lattice with large majority atoms. Figuratively speaking this prevents the jumping atom from 'seeing' beyond the barrier.

If A is less repulsive than B ($\Delta < 0$), the second term in equation (19) gives not E_M but $E_a = E_M - \Delta E/2$:

$$E_M - \frac{\Delta E}{2}(\mathrm{A}_\alpha \rightarrow \mathrm{V}_\beta) = \alpha_{\mathrm{FCC}} \boldsymbol{u}[(G^{\mathrm{AA}}_{zz} + \Delta)\mathbf{I}]^{-1}\boldsymbol{u}a^2 \approx \alpha_{\mathrm{FCC}}\tilde{G}^{-1}a^2 \qquad (\Delta < 0). \tag{20}$$

The large B atoms are a stronger perturbation with respect to a pure A lattice. The small jumping atom will, already at the equilibrium position, strongly feel the interaction with the vacancy in the β-sublattice.

The difference of the two cases $\Delta > 0$ and $\Delta < 0$ can be understood, considering the asymmetry between large and small defects mentioned in subsection 3.2. Similar to the case for a monatomic FCC lattice, a vacancy in a lattice of larger majority atoms ($\Delta > 0$) will only induce a small relaxation. The vacancy on the minority lattice will be comparatively large and the jumping atom will fit well into it. The saddle point is not affected by a volume expansion needed to create the anti-site defect. Consequently the saddle point will not be shifted from its position in the monatomic case and is given by the interaction with atoms forming the 'gate' and the split vacancy. The mainly chemical energy bias has only a minor effect. In this sense, the migrating atom does not 'see' beyond the saddle point. In the opposite case, $\Delta < 0$, the lattice is less stiff and there is an appreciable relaxation of the vacancy. Removing a large B atom causes appreciable distortions of the lattice. The jumping atom has to carry some lattice expansion along. Its effect on the migrational saddle point is not included in the Green function description which, therefore, gives only the contribution E_a.

A caveat has to be given as regards the validity of the relations obtained: the second terms in equations (19) and (20) reproduce the values of E_M and $E_M - \Delta E/2$ respectively only if ΔE is not too large compared to E_M. We estimate that $|\Delta E|$ has to be smaller than $E_M/2$.

3.5. The jump $B_\beta \rightarrow V_\alpha$

This case is completely analogous to the previous one. Obviously G^{AA} has to be replaced by G^{BB} and Δ by $-\Delta$, giving

$$E_M(\mathrm{B}_\beta \rightarrow \mathrm{V}_\alpha) = \alpha_{\mathrm{FCC}} \boldsymbol{u}[(G^{\mathrm{BB}}_{xx} - \Delta)\mathbf{I}]^{-1}\boldsymbol{u}a^2 \approx \alpha_{\mathrm{FCC}} G^{\mathrm{BB}\,-1}_{xx}\left(1 + \frac{\Delta}{G^{\mathrm{BB}}_{xx}}\right)a^2 \qquad (\Delta > 0) \tag{21}$$

and

$$E_M - \frac{\Delta E}{2}(\mathrm{B}_\beta \to \mathrm{V}_\alpha) = \alpha_{\mathrm{FCC}}\boldsymbol{u}[(G^{\mathrm{BB}}_{xx} - \Delta)\mathbf{I}]^{-1}\boldsymbol{u}a^2$$
$$\approx \alpha_{\mathrm{FCC}}G^{\mathrm{BB}\,-1}_{xx}\left(1 + \frac{\Delta}{G^{\mathrm{BB}}_{xx}}\right)a^2 \qquad (\Delta < 0). \tag{22}$$

The same caveat regarding the relative values of E_M and ΔE applies to these formulae: $|\Delta E|$ has to be smaller than $E_M/2$.

4. Computer simulations

For guidance and as a check we performed extensive simulations during the derivation of the different formulae. We employed molecular statics—see e.g. [19]—using crystallites of up to 1372 atoms (region I). These crystallites are embedded in a crystal (region II). Atoms in region I are allowed to relax under the influence of their mutual interaction and their interaction with the atoms of region II which are constrained to their ideal-lattice sites. The positions of the atoms in region I are determined by a minimization of the potential energy. This minimization is achieved by a mixture of a steepest-descent and the conjugate gradient techniques [20]. In order to determine energy profiles, additional geometrical constraints are built in. Because of the fixed boundary conditions, the Green function matrix elements for the perfect lattice are calculated not simply from (2) but from the Born–von Karman force constants using formula (5).

As the potentials describing the interaction potentials between atoms of the same type, we chose modified Morse and Lennard-Jones potentials smoothly cut off after the second and eighth neighbours, respectively. The potential parameters were chosen to fit the lattice constants, the bulk modulus and the vacancy formation energies of Ni, Cu, Al, Pd and Ag. As the potential describing the interactions between atoms of different types we chose the average of the two monatomic potentials. The lattice parameters of the compounds were calculated by energy minimization with respect to the atomic coordinates. Sixteen systems forming the $L1_2$ structures were built in this way. We would like to emphasize that we do not intend to reproduce the atomic interactions of real $L1_2$ compounds in this way. We only wanted to have potentials that stabilize the $L1_2$ phase, to verify the relations given in section 3 between the computed values of the migration energies and the Green function matrix elements, based on the assumption that those relations also hold for real compounds. Our model reproduced the computed migration energies within 10%, as long as ΔE was smaller than $E_M/2$.

Table 1. Calculated lattice parameters (in Å), perfect-lattice Green function matrix elements (in units of 10^{-2} m N^{-1}), migration energies and ΔE values for Ni_3Al and Cu_3Au obtained from molecular dynamics calculations using embedded-atom-method (EAM) potentials [21, 22] and values of E_M or $E_M - \Delta E/2$ (called E_a in tables 1 and 2 to improve the layout) deduced from our model. All the energies are in eV.

						$\mathrm{A}_\alpha \to \mathrm{V}_\alpha$	$\mathrm{A}_\alpha \to \mathrm{V}_\beta$			$\mathrm{B}_\beta \to \mathrm{V}_\alpha$		
		a	G^{AA}_{xx}	G^{AA}_{zz}	G^{BB}_{xx}	E_M	E_M	ΔE	E_a	E_M	ΔE	E_a
Ni_3Al	EAM	3.547	1.169	1.111	1.092	0.86	0.92	0.03	0.90	1.17	0.74	0.80
	Model					0.91	0.93			1.00		
Cu_3Au	EAM	3.757	1.740	2.527	1.687	0.55	0.43	−0.28	0.57	0.70	0.46	0.47
	Model					0.54			0.56			0.57

As an additional test of our formulae, we carried out subsequent simulations using embedded-atom-method (EAM) potentials for Ni_3Al and Cu_3Au [21,22]. We chose the EAM because we wanted to make a test with an interaction model with a very different structure. Again we calculated the different migration energies and Green functions and compared the energies with the ones deduced from our model. For Ni_3Al and Cu_3Au, Δ is positive and negative respectively, so all the variants of the formulae given in this section can be tested. The results are displayed in table 1. They show both the strengths and the limitations of our model. The values of E_M or $E_M - \Delta E/2$ for the $A_\alpha \rightarrow V_\alpha$ and $A_\alpha \rightarrow V_\beta$ jumps are well reproduced by our model; however, for both compounds, due to the relatively high values of ΔE ($\Delta E \approx 0.7 E_M$), our estimates of the energies for the $B_\beta \rightarrow V_\alpha$ jump deviate by about 20%.

5. Values of the migration energies and discussion

For those $L1_2$ compounds whose phonon dispersions have been measured, the perfect-lattice Green function matrix elements and the values of E_M or $E_M - \Delta E/2$, deduced from our model, are given in table 2. For the compounds considered here, those where Δ is positive (negative), i.e. compounds whose A–A repulsion is stronger (weaker) than the A–B one, are those whose majority atoms (A) are heavier (lighter) than the minority ones (B). We emphasize once again that our model gives good energy values for the two jumps $A_\alpha \rightarrow V_\beta$ and $B_\beta \rightarrow V_\alpha$ only if $|\Delta E|$ is smaller than $E_M/2$. Our model cannot predict whether this condition will be fulfilled.

Table 2. Critical temperatures of stability of the $L1_2$ phase, melting temperatures (in K), lattice parameters (in Å, from reference [41]), perfect-lattice Green function matrix elements (in units of 10^{-2} m N^{-1}) and values of E_M or $E_M - \Delta E/2$ (in eV) deduced from our model in section 3. For each $L1_2$ compound, the reference to where the Born–von Karman force constants used to calculate the Green function matrix have been found is given in the first column. All phonon dispersions (used to deduce the force constants) were measured at room temperature, except where otherwise stated.

							$A_\alpha \rightarrow V_\alpha$	$A_\alpha \rightarrow V_\beta$		$B_\beta \rightarrow V_\alpha$	
A_3B compound	T_C	T_M	a	G_{xx}^{AA}	G_{zz}^{AA}	G_{xx}^{BB}	E_M	E_M	E_a	E_M	E_a
Cu_3Au [36]	665	1225	3.743	1.872	2.603	1.773	0.52		0.53		0.55
Pd_3Fe [37] (80 K)	955	1655	3.85	1.264	0.929	1.553	0.97	1.14		0.90	
Fe_3Pt [38]	1095	1835	3.73	1.407	2.319	1.371	0.59		0.63		0.64
Pt_3Mn [39] (80 K)	1260	1820	3.90	0.923	0.699	2.077	1.37	1.58		0.65	
Ni_3Al [24]	1275	1670	3.589	1.202	1.185	1.172	0.90	0.91		0.93	
Pt_3Fe [38]	1575	1955	3.780	1.117	0.876	1.235	1.12	1.27		1.13	
Pd_3Ce [40]	1710	1710	4.112	1.624	1.863	1.262	0.82		0.82		1.03

Let us point out that, in the same way as for pure metals [8], our model gives temperature-dependent migration energies due to the temperature dependence of the phonon dispersions.

Other direct determinations of the migration energies in $L1_2$ intermetallics are scarce. Data exist for the widely studied Ni_3Al compound. Using the embedded-atom method, Foiles and Daw [23] calculated the migration energies 1.02, 0.91 and 1.28 eV for the $Ni_\alpha \rightarrow V_\alpha$, $Ni_\alpha \rightarrow V_\beta$ and $Al_\beta \rightarrow V_\alpha$ jumps respectively. The first two values agree with the ones from our model (see table 2). The third one deviates by 0.35 eV. This might be due to there being such a large bias for this jump (seen in our molecular dynamics calculations; see table 1) that our model is being used beyond its range of applicability. However, the real migration energy for this jump is certainly smaller than the one predicted in reference [23]. The vibrations of the Al atoms are mainly high-frequency optical modes [24]. Stassis *et al* [25] measured

those modes 2 THz below the ones calculated by Foils and Daw. In the framework of our model, which gives a large weight to the low-frequency modes, the real migration energy for the $Al_\beta \rightarrow V_\alpha$ jump should then be markedly reduced. The migration energy for the motion of a Ni vacancy has been estimated experimentally from positron annihilation studies after electron irradiation [7] as $E_M = 1.2 \pm 0.2$ eV. It is, within the uncertainty of our model (10%), in agreement with the value of 0.9 eV determined here for the $Ni_\alpha \rightarrow V_\alpha$ jump.

Several experimental (see e.g. references [26–28]) and theoretical [29, 30] results show that the ordering energy contributes significantly to the migration and formation energies in intermetallic compounds. For the migration energy, this dependency has been extensively studied by means of Monte Carlo simulations of the long-range ordering kinetics in $B2$ (or CsCl) and DO_3 (or Fe_3Al) phases [31–34]. The Monte Carlo model, based on a nearest-neighbour vacancy jump mechanism, relies on an Ising Hamiltonian with effective pair interaction energies for first- and second-nearest neighbours (V_1 and V_2). These energies determine the critical temperatures T_C of stability of the ordered structures. Keeping V_1 constant and varying the effective pair interaction energy ratio V_2/V_1 which is equivalent to changing T_C, one gets a significant contribution of the ordering energy to the mean migration energy ($\Delta\overline{E_M}/\Delta T_C = 0.5$ eV/1000 K). This result reproduces quantitatively the experimental trends for the activation energy for self-diffusion in equiatomic FeCo [26] and the mean migration energy in Fe_3Al and Fe_3Si compounds [14]. Even though we are not able to scale all of the migration energies obtained by our model to the same V_1-value (because the effective interactions are not known for all of the compounds considered here), it is nevertheless interesting to look at them as a function of T_C, the critical temperature of stability of the $L1_2$ phase. This function is shown in figure 4 for our values of E_M and $E_M - \Delta E/2$ determined at 300 K. For the three types of jump, we see a clear tendency for those energies to increase as a function of T_C, indicating that, in the $L1_2$ phase also, the ordering energy contributes significantly to the migration energies. Fitting the three sets of points to a straight line leads to similar values of $\Delta E_M/\Delta T_C$ (0.5 eV/1000 K) and similar intercepts of the $T_C = 0$ axis (0.2 eV) for the three jump types. As the migration energies have not been scaled to the same V_1-value in figure 4, we will not compare the thus-obtained value for $\Delta E_M/\Delta T_C$ to the one

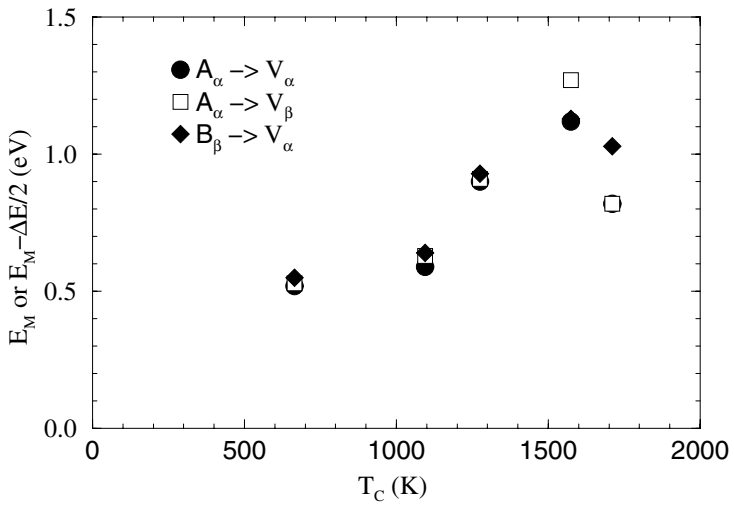

Figure 4. Values of E_M or $E_M - \Delta E/2$ at 300 K from table 2 displayed as a function of the critical temperature of stability of the $L1_2$ structure (T_C).

from the Monte Carlo simulations for $B2$ and DO_3 compounds. Monte Carlo simulations for $L1_2$ structures using the model as described above are currently being undertaken for this purpose [35].

6. Conclusions

We have shown that the migration energies for the three nearest-neighbour vacancy jumps in $L1_2$ compounds can be related to the measured phonon dispersions. As was done for pure metals (equation (1)), the energies are separated into a structural, material-independent term (α_{FCC}) and a material-dependent term (a combination of the perfect-lattice Green function matrix elements of the two constituent atoms). The compounds are separated into two groups depending on the relative size of the constituent atoms, Δ. In particular, for the two jump types where the migrating atom moves from one sublattice into the other (namely $\mathrm{A}_\alpha \rightarrow \mathrm{V}_\beta$ and $\mathrm{B}_\beta \rightarrow \mathrm{V}_\alpha$), inducing a difference between final and initial potential energies, the Green function matrix elements give access directly to E_M when the barrier that the migrating atom has to overcome is composed of majority atoms (A) larger than the minority ones ($\Delta > 0$), but only give access to $E_M - \Delta E/2$ in the opposite case ($\Delta < 0$). This reflects the fact that in the first case the lattice is mostly defined by larger majority atoms whereas in the opposite case the larger minority atoms are a strong perturbation. The short-range repulsive forces are in general the dominant ones in close-packed materials.

Our results should also help in the estimation of the relevant difference in energy associated with a vacancy–atom exchange in Monte Carlo simulations of atomic mobility. Up till now, two paths for evaluating the energy change have been followed. They are (i) taking the difference between the energies of the final and initial states [31, 42–44] and (ii) taking the saddle-point energy minus the initial energy [44–46], arguing that the system cannot 'know' *a priori* its energy behind the saddle point. Our present results show that the situation in $L1_2$ compounds is somewhat more complicated as it depends on which of the two types of atom is jumping.

Using our formulae, the values of E_M or $E_M - \Delta E/2$ have been calculated for $L1_2$ compounds whose phonon dispersions have been measured. For the cases of the $\mathrm{A}_\alpha \rightarrow \mathrm{V}_\beta$ and $\mathrm{B}_\beta \rightarrow \mathrm{V}_\alpha$ jumps, those energies are good estimates if ΔE, the difference in energy between the final state and the initial state, is not too large with respect to E_M. In the case of the Ni_3Al system, our model calculations are, within their range of application, in good agreement with other theoretical and experimental determinations. Comparing the values of E_M or $E_M - \Delta E/2$ for the compounds considered with the critical temperatures of stability of the $L1_2$ phase, we deduce that the ordering energy contributes significantly to the migration energy and with similar strength for the three types of jump.

For the monatomic systems it has been found that similar formulae hold for both the FCC and BCC structures [8]. A straightforward extension of our results for the close-packed $L1_2$ structure to the more open BCC-like $B2$ and DO_3 structures meets, however, with some difficulty. Relaxations seem to be more important and, depending strongly on the substance, they change the distance to the saddle point. To incorporate these effects in our formulae, more sophisticated calculations of both migration energies and phonon dispersions are needed.

Acknowledgment

We gratefully acknowledge P Ballone (University of Messina) for providing us with embedded-atom-method potentials for Ni_3Al and Cu_3Au and the molecular dynamics program to use them.

References

[1] Schaefer H E and Badura-Gergen K 1997 *Defect Diffusion Forum* **143–147** 193
[2] Würschum R, Grupp C and Schaefer H E 1995 *Phys. Rev. Lett.* **75** 97
[3] Wolff J, Franz M, Broska A, Kölher B and Hehenkamp T 1997 *Mater. Sci. Eng.* A **239+240** 213
[4] Würschum R, Badura-Gergen K, Kümmerle E A, Grupp C and Schaefer H E 1996 *Phys. Rev.* B **54** 849
[5] Schaefer H E, Frenner K and Würschum R 1999 *Phys. Rev. Lett.* **82** 948
[6] van Omnen A H and de Miranda J 1981 *Phil. Mag.* A **43** 387
[7] Wang T M, Shimotomai M and Doyama M 1984 *J. Phys. F: Met. Phys.* **14** 37
[8] Schober H R, Petry W and Trampenau J 1992 *J. Phys.: Condens. Matter* **4** 9321
Schober H R, Petry W and Trampenau J 1992 *J. Phys.: Condens. Matter* **5** 993 (corrigendum)
[9] Herzig C 1983 *Diffusion in Metals and Alloys (DIMETA-82)* ed F J Kedves and D L Beke (Zurich: Trans. Tech.) p 23
[10] Flynn C P 1968 *Phys. Rev.* **171** 682
[11] Squires G L 1978 *Introduction to the Theory of Thermal Neutron Scattering* (Cambridge: Cambridge University Press)
[12] Randl O G, Vogl G, Petry W, Hennion B, Sepiol B and Nembach K 1995 *J. Phys.: Condens. Matter* **7** 5983
[13] Randl O G 1994 *PhD Dissertation* University of Vienna
[14] Kentzinger E, Cadeville M C, Pierron-Bohnes V, Petry W and Hennion B 1996 *J. Phys.: Condens. Matter* **8** 5535
[15] Randl O G, Vogl G and Petry W 1996 *Physica* B **219+220** 499
[16] Leifried G and Breuer N 1978 *Point Defects in Metals I (Springer Tracts in Modern Physics vol 81)* ed G Höler (Berlin: Springer)
[17] Ehrhart P, Robrock K H and Schober H R 1986 *Physics of Radiation Effects in Crystals* ed R A Johnson and A N Orlov (Amsterdam: North-Holland) p 3
[18] Wollenberger H J 1993 *Materials Science and Technology* vol 1, ed R W Cahn, P Haasen and E J Kramer (Weinheim: Chemie) p 357
[19] Schober H R 1977 *J. Phys. F: Met. Phys.* **7** 1127
[20] Fletcher R and Reeves C M 1964 *Comput. J.* **7** 149
[21] Rubini S and Ballone P 1993 *Phys. Rev.* B **48** 99
[22] Foiles S M, Baskes M I and Daw M S 1986 *Phys. Rev.* B **33** 7983
[23] Foiles S M and Daw M S 1987 *J. Mater. Res.* **2** 5
[24] Fultz B, Anthony L, Nagel L J, Nicklow R M and Spooner S 1995 *Phys. Rev.* B **52** 3315
[25] Stassis C, Kayser F X, Loong C K and Arch D 1981 *Phys. Rev.* B **24** 3048
[26] Iijima Y and Lee C G 1995 *Acta Metall. Mater.* **43** 1183
[27] Tökei Z, Bernardini J, Gas P and Beke D L 1997 *Acta Mater.* **45** 541
[28] Kozubski R, Soltys J, Cadeville M C, Pierron-Bohnes V, Kim T H, Schwander P, Hahn J P, Kostorz G and Morgiel J 1993 *Intermetallics* **1** 139
[29] Schoijet M and Girifalco L A 1968 *J. Phys. Chem. Solids* **29** 481
[30] Schoijet M and Girifalco L A 1968 *J. Phys. Chem. Solids* **29** 497
[31] Yaldram K, Pierron-Bohnes V, Cadeville M C and Khan M A 1995 *J. Mater. Res.* **10** 591
[32] Kentzinger E 1996 *PhD Dissertation* University of Strasbourg
[33] Kentzinger E, Pierron-Bohnes V, Cadeville M C, Zemirli M, Bouzar H, Benakki M and Khan M A 1997 *Defect Diffusion Forum* **143–147** 333
[34] Kentzinger E, Zemirli M, Pierron-Bohnes V, Caseville M C, Bouzar H, Benakki M and Khan M A 1997 *Mater. Sci. Eng.* A **239+240** 784
[35] Cadeville M C *et al* 2000 in preparation
[36] Katano S, Iizumi M and Noda Y 1988 *J. Phys. F: Met. Phys.* **18** 2195
[37] Stirling W G, Cowley R A and Stringfellow M W 1972 *J. Phys. F: Met. Phys.* **2** 421
[38] Noda Y, Endoh T, Katano S and Iizumi M 1983 *Physica* B **120** 317
[39] Paul D M^{c}K, Cowley R A and Lucas B W 1979 *J. Phys. F: Met. Phys.* **9** 39
[40] Loong C K, Zarestky J, Stassis C, McMasters O D and Nicklow R M 1988 *Phys. Rev.* B **38** 7365
[41] Predel B 1991 *Landolt–Börnstein New Series* Group IV, vol 5, ed O Madelung (Berlin: Springer)
[42] Binder K and Khalos M H 1979 *Monte Carlo Methods in Statistical Physics* ed K Binder (Berlin: Springer)
[43] Vives E and Planes E 1993 *Phys. Rev.* B **47** 2557
[44] Weinkamer R, Fratzl P, Sepiol B and Vogl G 1998 *Phys. Rev.* B **58** 3082
[45] Fultz B 1987 *J. Chem. Phys.* **88** 3227
[46] Athènes M, Bellon P, Martin G and Haider F 1996 *Acta Mater.* **44** 4739